# Spatial versus temporal laser speckle contrast analyses in the presence of static optical scatterers

Julio C. Ramirez-San-Juan
Caitlin Regan
Beatriz Coyotl-Ocelotl
Bernard Choi

# Spatial versus temporal laser speckle contrast analyses in the presence of static optical scatterers

**Julio C. Ramirez-San-Juan,**[a,b,]* **Caitlin Regan,**[b,c] **Beatriz Coyotl-Ocelotl,**[a] **and Bernard Choi**[b,c,d]
[a]Instituto Nacional de Astrofisica, Optica y Electronica, Departamento de Optica, Luis Enrique Erro No. 1, Tonantzintla, Puebla 72840, Mexico
[b]University of California, Irvine, Beckman Laser Institute and Medical Clinic, Department of Surgery, 1002 Health Sciences Road East, Irvine, California 92612, United States
[c]University of California, Irvine, Department of Biomedical Engineering, 3120 Natural Sciences II, Irvine, California 92697, United States
[d]University of California, Irvine, Edwards Lifesciences Center for Advanced Cardiovascular Technology, 2400 Engineering Hall, Irvine, California 92697, United States

**Abstract.** Previously published data demonstrate that the temporal processing algorithm for laser speckle contrast imaging (LSCI) can improve the visibility of deep blood vessels and is less susceptible to static speckle artifacts when compared with the spatial algorithm. To the best of our knowledge, the extent to which the temporal algorithm can accurately predict the speckle contrast associated with flow in deep blood vessels has not been quantified. Here, we employed two phantom systems and imaging setups (epi-illumination and transillumination) to study the contrast predicted by the spatial and temporal algorithms in subsurface capillary tubes as a function of the camera exposure time and the actual flow speed. Our data with both imaging setups suggest that the contrast predicted by the temporal algorithm, and therefore the relative flow speed, is nearly independent of the degree of static optical scattering that contributes to the overall measured speckle pattern. Collectively, these results strongly suggest the potential of temporal LSCI at a single-exposure time to assess accurately the changes in blood flow even in the presence of substantial static optical scattering. © *2014 Society of Photo-Optical Instrumentation Engineers (SPIE)* [DOI: 10.1117/1.JBO.19.10.106009]

## 1 Introduction

Laser speckle contrast imaging (LSCI) is an optical technique based on calculating the contrast of an integrated speckle pattern, which allows us to analyze the dynamics of blood flow.[1] LSCI has attracted attention because it is able to image blood flow in skin,[2] retina,[3] and brain[4] at relatively high spatial and temporal resolutions and without the need for scanning of the region of interest. Additionally, it is simple and inexpensive relative to similar laser Doppler-based techniques.[5,6] During the last decade, the theoretical model behind LSCI has evolved to include modifications to the original Fercher and Briers model,[7] taking into account the effects of static optical scatterers,[8,9] as well as the ratio of pixel and speckle sizes,[10–13] resulting in the following speckle imaging equation:

$$K_{i,j} = \alpha^{1/2} \left[ \sqrt{\frac{1}{M}} \mathrm{erf}\left(\sqrt{\pi M}\right) - \left(\frac{1}{\pi M}\right)\left(1 - e^{-\pi M}\right) \right]$$
$$\times \left[ \rho_{i,j}^2 \frac{e^{-2x_{i,j}} - 1 + 2x_{i,j}}{2x_{i,j}^2} + 4\rho_{i,j}(1 - \rho_{i,j}) \frac{e^{-x_{i,j}} - 1 + x_{i,j}}{x_{i,j}^2} \right.$$
$$\left. + (1 - \rho_{i,j})^2 \right]^{1/2} + K_{\mathrm{noise}}, \qquad (1)$$

where $K_{i,j}$ is the local contrast of the raw speckle image at the pixel $(i, j)$; $\alpha$ is a normalization parameter; $M$ is the area of the pixel divided by the diffraction-limited area of the minimally resolvable speckle; $\rho_{i,j}$ is the fraction of light reaching the pixel $(i, j)$ that interacts with moving optical scatterers; and $x_{i,j} = T/\tau_C$, where $T$ is the exposure time of the CCD camera and $\tau_C$ is the correlation time of the light intensity.

Research groups proposed various approaches to calculate the speckle contrast from a raw speckle image or set of images.[14] Spatial analysis,[15] probably the most common approach, implements a sliding, square structuring element of $5 \times 5$ or $7 \times 7$ pixels to calculate the local speckle contrast $K$ as the standard deviation of pixel intensities ($\sigma$) divided by the mean intensity ($I$) within the element boundaries. Ideally, the speckle area should be at least twice the pixel area[10] to minimize detrimental effects because of spatial integration of the speckle pattern;[11] otherwise, a correction factor should be applied to the measured speckle contrast.[13] The spatial algorithm requires only one raw speckle image to compute a contrast image, and therefore offers high-temporal resolution at the expense of spatial resolution because of the use of the structuring element. To circumvent the reduction in spatial resolution, Cheng et al.[16] proposed a temporal algorithm that calculates a speckle contrast image by computing $K$ for each pixel across a sequence of images. This approach requires a minimum of 15 statistically independent images[16] and is associated with better spatial resolution at the expense of temporal resolution.

Recent studies describe results that support the use of the temporal algorithm to analyze raw speckle images. We discovered

*Address all correspondence to: Julio C. Ramirez-San-Juan, E-mail: jcram@inaoep.mx

that the temporal algorithm is more accurate than the spatial algorithm at assessing the relative change in flow speed.[12] This improved accuracy appears to be from the reduction in sensitivity of temporal analysis to the presence of static optical scatterers.[8,9,17] Li et al.[18] reported that the temporal algorithm enabled visualization of subsurface (>1 mm) blood vessels through the intact rat skull; these vessels were not visible in spatial speckle contrast images. Here, we report on *in vitro* experiments that extend upon our understanding of temporal speckle contrast analysis. Specifically, we focused on the quantitation of speckle contrast and the impact of depth of fluid flow on speckle contrast values. We studied these effects using two clinically relevant imaging geometries: epi-illumination and transillumination.

## 2 Materials and Methods

We used two separate phantom setups for the experiments described in this paper: (1) an epi-illuminated skin-simulating phantom (Fig. 1), and (2) a transilluminated excised human tooth (Fig. 2).

### 2.1 Skin-Simulating Phantom

We constructed the skin-simulating phantom using a silicone block containing appropriate concentrations of $TiO_2$ to mimic the reduced scattering coefficient ($1\ mm^{-1}$) of biological tissue at visible and near-infrared wavelengths (Fig. 1). We embedded a glass capillary tube, with an inner diameter of 550 $\mu m$, at the surface of the block. We placed a second thin silicone skin-simulating phantom of varying thicknesses (190 to 1000 $\mu m$) on top of the block to mimic the overlying tissue. We fabricated the thin phantoms using $TiO_2$ powder and coffee to simulate the optical scattering and absorption coefficients, respectively, of the epidermis.[19] By using different thicknesses of the overlying layer, we effectively modulated $\rho$.

For laser speckle imaging (LSI) with epi-illumination, we used an 808-nm laser (Ondax, Monrovia, California) as the excitation source, with a variable attenuator to adjust the intensity of illumination and ground-glass diffuser to expand and homogenize the incident laser light (spot illumination: 5-mm diameter). A Retiga EXi FAST cooled CCD camera (QImaging, Surrey, BC, Canada) collected the raw speckle images at 20 fps. The camera was equipped with a macrolens (Nikon, Melville, New York), with an aperture setting of $f/4$. We acquired images
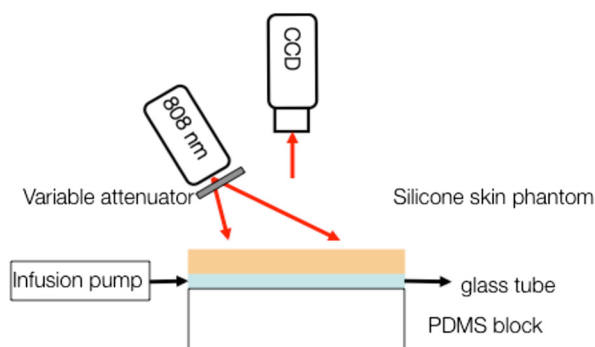
using Q-Capture Pro v5.1 software and selected the exposure time using the autoexpose function. We collected images of the phantom at exposure times ranging between 66 $\mu s$ and 43 ms by using the variable attenuator to change the irradiance of the excitation light. We collected data from the phantom with the following configurations: no top layer present (i.e., microchannel at surface of phantom) and with overlying top-layer thicknesses (TLTs) of 190 m, 310, 510, and 1000 $\mu m$. We used a syringe pump (Harvard Apparatus, Holliston, Massachusetts) to infuse 5% Intralipid solution as a blood surrogate (Baxter Healthcare, Deerfield, Illinois) into the channel at speeds of 0 to 18 mm/s.

### 2.2 Tooth-Simulating Phantom

We also simulated transillumination LSI conditions, recently proposed by Stoianovici et al.,[20] for the study of pulpal blood flow in teeth (Fig. 2). Teeth are well suited for transillumination LSI because of the highly forward scattering feature of interior dentine tubules.[21] We used an excised human adult molar as a phantom. We drilled a small hole from the middle of the occlusal surface of the tooth to the bottom of the tooth between the roots. We inserted a Tygon tube with an inner diameter of 250 $\mu m$ into the hole and connected it to a syringe pump.

Our experimental setup consisted of a configuration currently under investigation for study of pulpal blood flow. We illuminated the tooth on one side with a fiber-coupled 632.8-nm HeNe laser (JDSU, Milpitas, California). On the opposite side of the tooth, we positioned a leached fiber bundle (Schott, Southbridge, Massachusetts)[22] with a drum lens to focus the image on to a CCD camera (Flea3, Point Gray, Richmond, BC, Canada). We acquired images with FlyCap software (Point Gray) at a fixed exposure time of 10 ms and a gain of 24 dB. For this experiment, we calculated spatial and temporal contrasts in two regions of interest, one on the left side of the tooth and the other on the right. The tooth was approximately 300-$\mu m$ thicker on the right side than the left, effectively resulting in different $\rho$ at the two interrogated regions.

With both experimental setups, we collected a sequence of 30 images per experimental condition and processed with both spatial and temporal speckle imaging algorithms. With the spatial algorithm, we used a sliding $7 \times 7$ pixel structuring element to calculate maps of speckle contrast from each acquired raw speckle image and obtained a final contrast image by averaging the 30 contrast images.[15] We calculated temporal contrast on a pixel-by-pixel basis, across all 30 images in the sequence.[16] All values shown in the data figures (Figs. 3–6) represent the average contrast in a region of interest ($20 \times 100$ pixels) positioned over the center of the tube.



**Fig. 1** Experimental setup used for epi-illumination experiments. We infused 5% Intralipid into a glass capillary tube embedded at different depths from the surface of a two-layer silicone phantom geometry. We used epi-illumination with an 808-nm laser and collected raw speckle images with a cooled CCD camera.
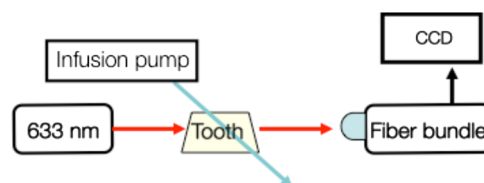


**Fig. 2** Experimental setup used for transillumination experiments. We infused Intralipid through Tygon tubing threaded through the tooth model. We transilluminated the tooth with a 632.8-nm laser and collected images with a CCD camera via a fiber bundle.
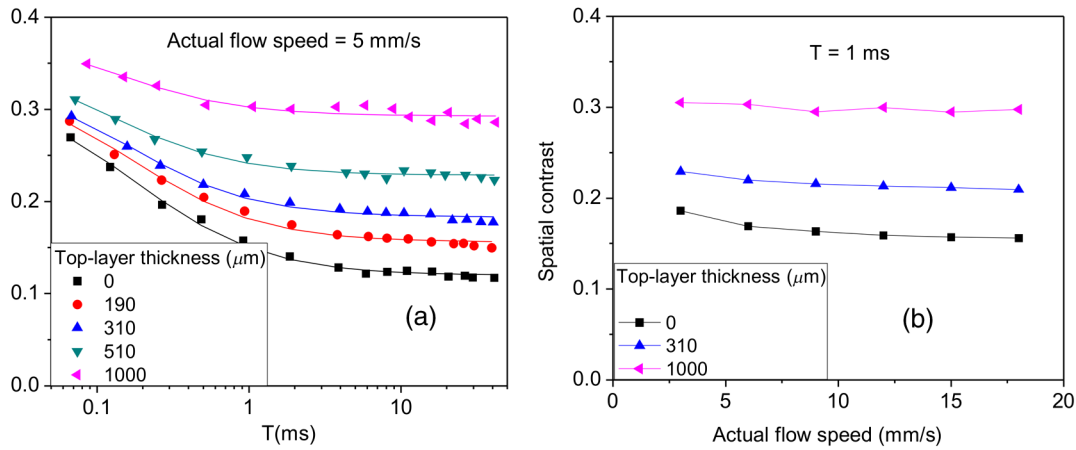
**Fig. 3** (a) Spatial speckle contrast increased with increasing top-layer thickness (TLT) at a given exposure time ($T$). The symbols represent the experimental data and the continuous lines data fits using Eq. (1). (b) At $T = 1$ ms, for a given actual flow speed value, spatial speckle contrast increased with increasing TLT.

## 3 Results and Discussion

### 3.1 *Skin-Simulating Phantom*

Similar to previously published data,[8] for a given TLT, we observed that the spatial speckle contrast decreased with an increase in $T$ [Fig. 3(a)]. For a given $T$, with an increase in TLT, the contrast increased because of a decrease in $\rho$. For a given flow speed, the contrast increased with an increase in TLT [Fig. 3(b)]. Collectively, these data demonstrate that, for flow in a subsurface tube, the spatial speckle contrast analysis is incapable of enabling unambiguous assessment of flow speed within the tube.

For a given TLT [Fig. (3a)], the spatial speckle contrast was maximum ($K_M$) at the shortest $T$, and then asymptotically decayed to a minimum ($K_m$). For a given $T$, the dynamic range of spatial speckle contrast (i.e., $\Delta K = K_M - K_m$) decreased with increasing TLT, because of a corresponding decrease in $\rho$. We fit Eq. (1) to the experimental data in Fig. 3(a) to estimate

$\tau_C$, $\rho$, and $K_m$. From the fitting results, the mean value of $\tau_C$ was $61.0 \pm 5.9$ $\mu$s, which is similar to the values reported by Parthasarathy et al.[8] for similar flow speed. $\rho$ and $K_m$ are plotted versus TLT in Fig. 4. For a given actual flow speed, we observe an exponential decay of $\rho$ with an increase in TLT [Fig. 4(a)], which we postulate is associated with the exponential behavior of light attenuation described by Beer's law. Because of the asymptotic behavior of $K_m$ with increasing $T$ (and hence increasing $x$), we determine $K_m$ as

$$K_m = \operatorname*{Lim}_{x \to \infty} K$$
$$= \alpha^{1/2} \left[ \sqrt{\frac{1}{M}} \operatorname{erf}\left( \sqrt{\pi M} \right) - \left( \frac{1}{\pi M} \right)\left( 1 - e^{-\pi M} \right) \right]$$
$$\times (1 - \rho) + K_{\text{noise}}, \quad (2)$$

where $\rho \; \epsilon \; [0,1]$. From Eq. (2), we see that $K_m$ decreases in a linear fashion with a decrease in TLT [Fig. 4(a)]. From the
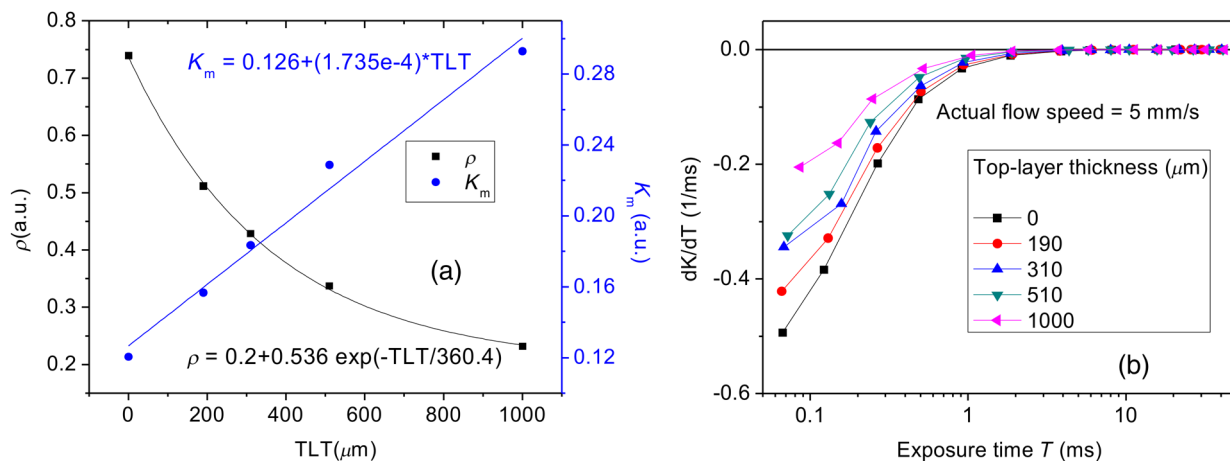


**Fig. 4** Spatial speckle contrast depends strongly on the fraction of nonmoving optical scatterers (e.g., $1-\rho$) and hence on the TLT. (a) $\rho$ decreases in exponential fashion with TLT, and $K_m$ increases in linear fashion with TLT. Solid points represent the experimental data, and lines represent the fits to the data. (b) The sensitivity of $K$ to exposure time $T$ depends strongly on TLT, for short $T$ (<1 ms), the sensitivity decreases for thicker TL and for $T > 1$ ms, the expected value of the contrast is constant [see Fig. 3(a)] and therefore the sensitivity approaches to zero.
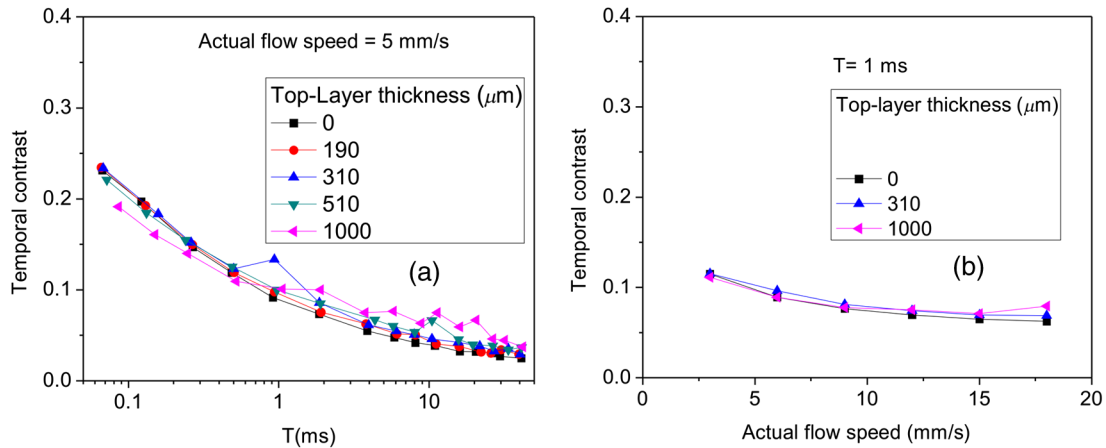
**Fig. 5** Temporal contrast versus $T$ (a) and versus actual flow speed (b) with different TLTs. The temporal processing scheme gives a more consistent measurement of contrast regardless of the presence of a static scattering layer.

first derivative of Eq. (1), we see that the sensitivity of spatial speckle contrast ($dK/dT$) decreases with an increase in TLT [Fig. 4(b)]. Collectively, our experimental data and analysis using Eq. (1) demonstrate that the spatial speckle contrast has a strong dependence on the fraction of nonmoving optical scatterers (e.g., $1 - \rho$), which in turn depends on the TLT. Hence, spatial speckle contrast analysis is incapable of accurate quantitation of subsurface flow dynamics because of the impact of TLT on $K$.

Previous reports[8,12,18] present data that strongly suggest that the temporal speckle contrast is altered primarily by temporal variations in light remitted from the sample and considerably less sensitive to static optical scatterers. We set out to determine the degree to which temporal contrast depends on specific independent variables. We find that the temporal contrast decreases with increasing $T$ [Fig. 5(a)] and increasing flow speed [Fig. 5(b)], but we also observed that the contrast is relatively independent of TLT for a wide range of values (0 to 1000 $\mu$m; Fig. 5).

### 3.2 Tooth-Simulating Phantom

We also studied this relationship using a transillumination LSI configuration, a setup previously proposed for study of teeth[20]
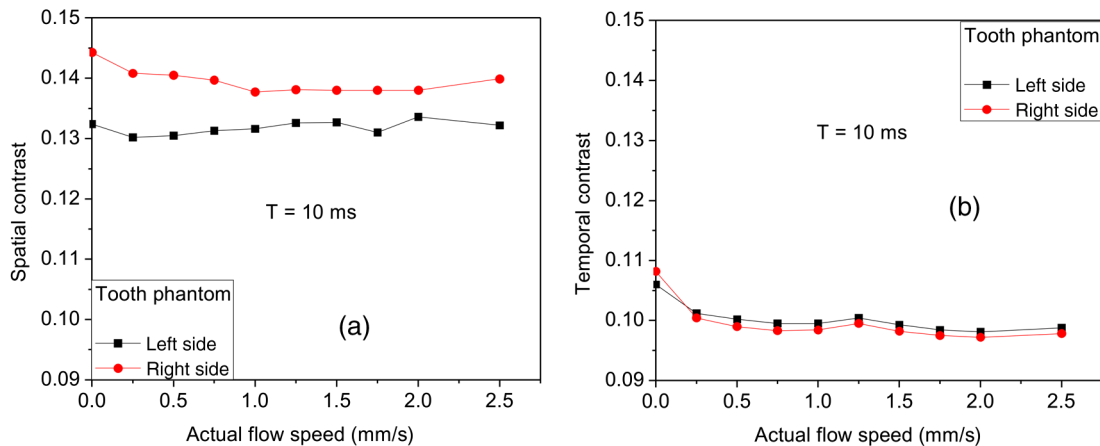
and joints,[23] and used routinely by our group to assess the blood flow in the rodent dorsal window chamber model.[24] We used a tooth model in which the thickness of the right side of the tooth was approximately 300-$\mu$m thicker than the left side, resulting in a higher proportion of static scatterers (i.e., lower $\rho$). Similar to the data collected with the epi-illumination setup, we observed that the spatial contrast depends on TLT [Fig. 6(a)], and temporal contrast is independent of TLT [Fig. 6(b)].

In this work, we studied the impact of overlying optical scatterers on measurements of speckle contrast. We used two different imaging setups and both spatial and temporal contrast analyses. With spatial analysis and epi-illumination, we determined that the speckle contrast offset $K_m$ increases in a linear fashion with TLT [Fig. 4(a)] and the sensitivity of speckle contrast decreased with an increase in TLT [Fig. 4(b)]. With temporal speckle contrast analysis (Fig. 5), speckle contrast measurements were remarkably independent of TLT, presumably due to the relative immunity of temporal contrast to contributions from static optical scatterers.[16–18] Our data demonstrate that the temporal contrast analysis can characterize accurately speckle contrast because of subsurface moving scatterers for TLT as thick as 1 mm, and for a wide range of $T$ and flow speeds. We observed similar results with a transillumination



**Fig. 6** Spatial versus temporal contrast in different regions of interest on a tooth (different thicknesses) as a function of flow speed.

geometry. Collectively, these results strongly suggest the potential of temporal LSI at a single-exposure time to assess the changes in blood flow even in the presence of substantial static optical scattering, which can ultimately be combined with methods to improve the localization of speckle contrast such as spatial frequency domain[25,26] or magnetomotive techniques.[27]

## References

1. A. F. Fercher and J. D. Briers, "Flow visualization by means of single-exposure speckle photography," *Opt. Commun.* **37**(5), 326–330 (1981).
2. B. Choi, N. M. Kang, and J. S. Nelson, "Laser speckle imaging for monitoring blood flow dynamics in the in vivo rodent dorsal skin fold model," *Microvasc. Res.* **68**(2), 143–146 (2004).
3. Y. Tamaki et al., "Noncontact, two-dimensional measurement of tissue circulation in choroid and optic nerve head using laser speckle phenomenon," *Exp. Eye Res.* **60**(4), 373–383 (1995).
4. A. K. Dunn et al., "Dynamic imaging of cerebral blood flow using laser speckle," *J. Cereb. Blood Flow Metab.* **21**, 195–201 (2001).
5. K. Yaoeda et al., "Measurement of microcirculation in the optic nerve head by laser speckle flowgraphy and scanning laser Doppler flowmetry," *Am. J. Ophthalmol.* **129**(6), 734–739 (2000).
6. C. Riva, B. Ross, and G. B. Benedek, "Laser Doppler measurements of blood flow in capillary tubes and retinal arteries," *Invest. Ophthalmol.* **11**(11), 936–944 (1972).
7. R. Bandyopadhyay et al., "Speckle-visibility spectroscopy: a tool to study time-varying dynamics," *Rev. Sci. Instrum.* **76**, 093110 (2005).
8. A. B. Parthasarathy et al., "Robust flow measurement with multi-exposure speckle imaging," *Opt. Express* **16**(3), 1975–1989 (2008).
9. D. A. Boas and A. K. Dunn, "Laser speckle contrast imaging in biomedical optics," *J. Biomed. Opt.* **15**(1), 011109 (2010).
10. S. J. Kirkpatrick, D. D. Duncan, and E. M. Wells-Gray, "Detrimental effects of speckle-pixel size matching in laser speckle contrast imaging," *Opt. Lett.* **33**(24), 2886–2888 (2008).
11. O. Thompson, M. Andrews, and E. Hirst, "Correction for spatial averaging in laser speckle contrast analysis," *Biomed. Opt. Express* **2**(4), 1021–1029 (2011).
12. J. C. Ramirez-San-Juan et al., "Effects of speckle/pixel size ratio on temporal and spatial speckle-contrast analysis of dynamic scattering systems: implication for measurements of blood-flow dynamics," *Biomed. Opt. Express* **4**(10), 1883–1889 (2013).
13. J. C. Ramirez-San-Juan et al., "Simple correction factor for laser speckle imaging of flow dynamics," *Opt. Lett.* **39**(3), 678–681 (2014).
14. M. Draijer et al., "Review of laser speckle contrast techniques for visualizing tissue perfusion," *Lasers Med. Sci.* **24**(4), 639–651 (2009).
15. J. D. Briers and S. Webster, "Quasi real-time digital version of single-exposure speckle photography for full-field monitoring of velocity or flow fields," *Opt. Commun.* **116**(1–3), 36–42 (1995).
16. H. Cheng et al., "Modified laser speckle imaging method with improved spatial resolution," *J. Biomed. Opt.* **8**(3), 559–564 (2003).
17. H. Cheng, Y. Yan, and T. Q. Duong, "Temporal statistical analysis of laser speckle images and its application to retinal blood-flow imaging," *Opt. Express* **16**(14), 10214–10219 (2008).
18. P. Li et al., "Imaging cerebral blood flow through the intact rat skull with temporal laser speckle imaging," *Opt. Lett.* **31**(12), 1824–1826 (2006).
19. R. B. Saager et al., "Multi-layer silicone phantoms for the evaluation of quantitative optical techniques in skin imaging," *Proc. SPIE* **7567**, 756706 (2010).
20. C. Stoianovici, P. Wilder-Smith, and B. Choi, "Assessment of pulpal vitality using laser speckle imaging," *Lasers Surg. Med.* **43**(8), 833–837 (2011).
21. S. Kakino, Y. Takagi, and S. Takatani, "Absolute transmitted light plethysmography for assessment of dental pulp vitality through quantification of pulp chamber hematocrit by a three-layer model," *J. Biomed. Opt.* **13**(5), 054023 (2008).
22. S. K. Nadkarni et al., "Laser speckle imaging of atherosclerotic plaques through optical fiber bundles," *J. Biomed. Opt.* **13**(5), 054016 (2008).
23. J. F. Dunn et al., "A transmissive laser speckle imaging technique for measuring deep tissue blood flow: an example application in finger joints," *Lasers Surg. Med.* **43**(1), 21–28 (2011).
24. A. J. Moy et al., "Wide-field functional imaging of blood flow and hemoglobin oxygen saturation in the rodent dorsal window chamber," *Microvasc. Res.* **82**(3), 199–209 (2011).
25. A. Mazhar et al., "Wavelength optimization for rapid chromophore mapping using spatial frequency domain imaging," *J. Biomed. Opt.* **15**(6), 061716 (2010).
26. T. B. Rice et al., "Quantitative, depth-resolved determination of particle motion using multi-exposure, spatial frequency domain laser speckle imaging," *Biomed. Opt. Express* **4**(12), 2880–2892 (2013).
27. J. Kim, J. Oh, and B. Choi, "Magnetomotive laser speckle imaging," *J. Biomed. Opt.* **15**(1), 011110 (2010).

Biographies of the authors are not available.